On Tungstates of Divalent Cations (I) – Structural Investigation and Spectroscopic Properties of $Sr_2[WO_5]$ and $Ba_2[WO_5]$

Stephan G. Jantz,[a] Florian Pielnhofer,[b] Marwin Dialer,[a] and Henning A. Höppe*[a]

Dedicated to Professor Thomas Schleid on the Occasion of his 60th Birthday

Abstract. The crystal structures of $Sr_2[WO_5]$ [$Pna2_1$, $a = 7.2457(3)$ Å, $b = 10.8867(5)$ Å, $c = 5.5391(3)$ Å, $Z = 4$, $R_{int} = 0.0671$, $R_1 = 0.0495$, $wR_2 = 0.0462$] and $Ba_2[WO_5]$ [$Pnma$, $a = 7.3828(2)$ Å, $b = 5.71420(10)$ Å, $c = 11.4701(3)$ Å, $Z = 4$, $R_{int} = 0.0294$, $R_1 = 0.0146$, $wR_2 = 0.0284$] are revised, based on single-crystal XRD data. Furthermore spectroscopic data (infrared, Raman, and UV/Vis) assisted by DFT calculations are discussed and first results on the luminescence properties of $Sr_2[WO_5]$:Eu^{3+} are presented.

Introduction

In the course of our systematic investigations on phosphors[1–4] we also shed light on tungstates, e.g. $Na_2RE(PO_4)$ (WO_4) (RE = Y, Tb – Lu),[5] which are known to be excellent sensitizers for rare earth luminescence. In such phosphors tungstate ions can be excited by highly-efficient charge-transfer transitions and ideally transfer this energy onto adjacent rare-earth ions such as Eu^{3+} or Tb^{3+}.[5,6]

Recently, the crystal structure of $Sr_2[WO_5]$ was described by *Keskar* et al.[7] in the space group *Pnma* (no. 62), applying X-ray and neutron powder diffraction techniques. Yet in 1974, *Shevchenko* et al.[8] described $Sr_2[WO_5]$ and $Ba_2[WO_5]$ being isostructural, suggesting the orthorhombic space groups *Pnma* or $Pna2_1$ on the basis of *Laue* photographs of $Ba_2[WO_5]$ single crystals. The authors also indexed the powder diffraction pattern of $Sr_2[WO_5]$, quoted the lattice parameters of $Ba_2[WO_5]$ and suggested the structure to consist of "infinite chains of tungsten-oxygen octahedra connected by their vertices". The crystal structure of $Ba_2[WO_5]$ was finally revealed by *Kovba* et al. via single crystal X-ray diffraction.[9]

Gateshki and *Igartua*[10] observed $Sr_2[WO_5]$ as side phase in Sr_2MWO_6 (M = Ca, Mg) and involved it into their Rietveld refinement. Therefore they investigated the structural details of $Sr_2[WO_5]$ by means of Rietveld refinement,[11] starting from the structural model of $K_2VO_2F_3$,[12] as suggested by *Kovba* et al.[9] and noted in PDF-card no. 00–025–0810.[13] While their refinement in space group *Pnma* yielded unusual isotropic dis-

* Prof. Dr. H. A. Höppe
  E-Mail: henning@ak-hoeppe.de
[a] Lehrstuhl für Festkörperchemie
  Universität Augsburg
  Universitätsstraße 1
  86159 Augsburg, Germany
[b] Abteilung Nanochemie
  Max-Planck-Institut für Festkörperforschung
  Heisenbergstr. 1
  70569 Stuttgart, Germany

placement parameters (cf. Table S1, Supporting Information), using space group $Pna2_1$ resulted in insignificant better values. The structural data presented by *Keskar* et al.[7] also show extremely large anisotropic displacement parameters for the oxygen atoms in relation to those of strontium and tungsten pointing clearly towards some inconsistencies of the structure model.

We revised the crystal structure of $Sr_2[WO_5]$ based on single-crystal X-ray diffraction data to address these strange extremely large displacement parameters and compare it to that of $Ba_2[WO_5]$, for which we present full crystal data for the first time. Moreover, we present first spectroscopic results on both title compounds supported by theoretical calculations to assess the suitability of these compounds to act as host structures for sensitized phosphors.

Results and Discussion

At first glance the structure solution in *Pnma* (suggested by XPREP) appeared reasonable, resulting in very good residuals of $R_1 = 0.0119$ and $wR_2 = 0.0213$. A closer look on the displacement parameters showed the same unusual values obtained earlier by others. The anisotropic displacement ellipsoids comprise an extreme cigar-shape behavior (Figure 1), also apparent from the principal mean square atomic displacements (Table 1).

These cigars suggest the introduction of split positions. Nevertheless in this case only the terminal oxygen atom OT3 splits into crystallographically distinct sites, whereas the split positions of bridging OB and terminal OT1 and OT2 are generated by symmetry. This can be healed by reduction to the lower symmetric space group $Pna2_1$ and introduction of a respective twin law. Thereby the displacement ellipsoids of the oxygen atoms (Figure 3) obtain more reasonable values (Table 2). The obtained batch scaling factor (BASF) of 0.49(3) reveals equal amounts of both twin domains within margin of error. Due to the absence of superstructure reflections or any indication for the presence of further domains in the precession images cal-
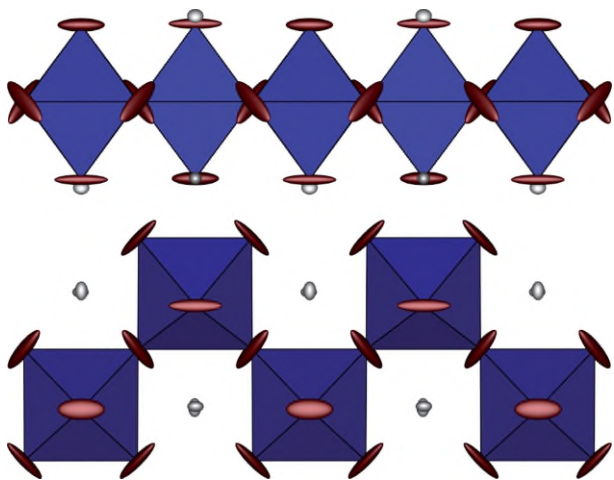
Figure 1. Side (top) and top (bottom) view of the WO_6 chains in $Sr_2[WO_5]$ in *Pnma*. Strontium grey, oxygen red, WO_6 octahedra blue; all atoms are drawn with their displacement ellipsoids at a 95% probability level. The displacement ellipsoids of the oxygen atoms comprise a suspicious "cigar shape".

Table 1. Principal mean square atomic displacements /$Å^2$ in $Sr_2[WO_5]$ in the *Pnma* structure solution.

Atom	$<u_x^2>$	$<u_y^2>$	$<u_z^2>$
Sr1	0.0057	0.0044	0.0029
Sr2	0.0070	0.0036	0.0034
W1	0.0031	0.0028	0.0021
OB	0.0808	0.0057	0.0034
OT1	0.0408	0.0094	0.0032
OT2	0.0523	0.0044	0.0012
OT3	0.0715	0.0067	0.0031

culated from the single-crystal diffraction data, we assume that both orientations are distributed in domains of almost equal amounts with no ordering. We suggest *Pna*2$_1$ to be the adequate space group to describe the structure of $Sr_2[WO_5]$.

Table 2. Principal mean square atomic displacements /$Å^2$ in $Sr_2[WO_5]$ in the *Pna*2$_1$ structure solution.

Atom	$<u_x^2>$	$<u_y^2>$	$<u_z^2>$
Sr1	0.0053	0.0034	0.0018
Sr2	0.0066	0.0048	0.0007
W1	0.0027	0.0017	0.0015
O1	0.0115	0.0066	0.0045
O2	0.0116	0.0054	0.0046
O3	0.0116	0.0054	0.0046
O4	0.0116	0.0054	0.0046
O5	0.0116	0.0054	0.0046

Crystal Structure Description in Pna2$_1$

To obtain the standard setting of *Pna*2$_1$, we interchanged the *b* and *c* axes with respect to the previous solution in space group *Pnma*, resulting in lattice parameters of $a = 7.2457(3)$ Å, $b = 10.8867(5)$ Å, and $c = 5.5391(3)$ Å. The crystal structure

(Figure 2) is built up by corner-sharing distorted WO_6 octahedra, forming infinite zigzag chains along the [001] direction. These chains are tilted relatively to the (010) plane, alternating in [010] direction (Figure 2 and Figure 3). The WO_6 octahedron exhibits an out-of-centre distortion, which is observed frequently in octahedrally coordinated d^0 transition metals.[14] It is surrounded by eleven strontium atoms forming a threefold capped distorted cube (Figure 4). Consequently, the W–O distances and O–W–O angles vary markedly in the ranges of
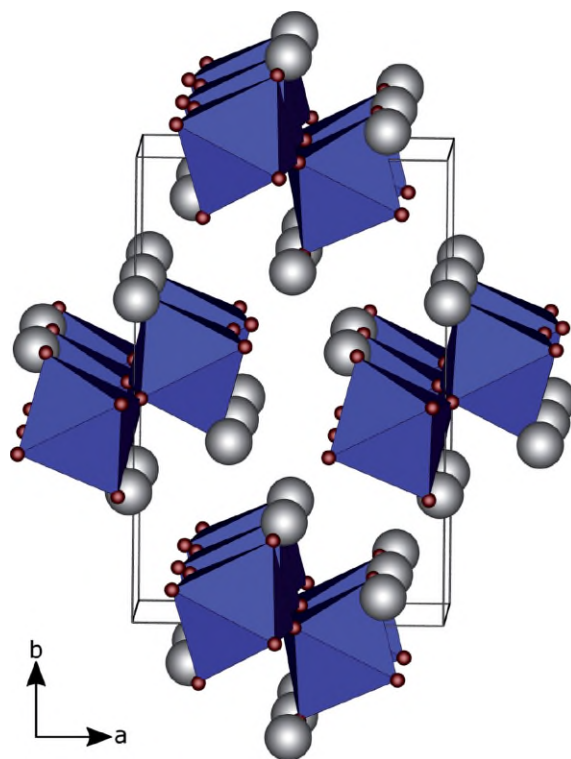
Figure 2. The crystal structure of $Sr_2[WO_5]$ in *Pna*2$_1$ (strontium grey, oxygen red, WO_6 octahedra blue).
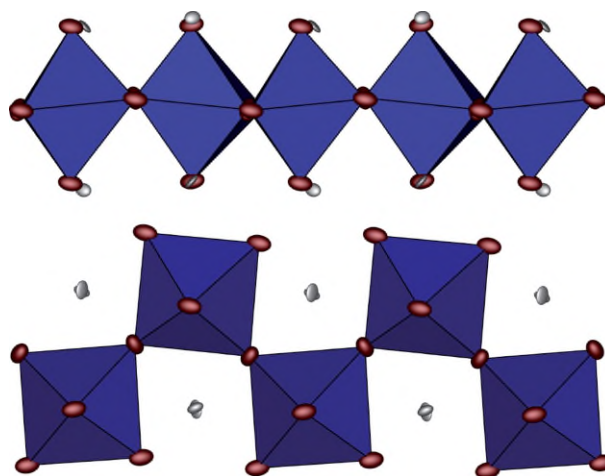
Figure 3. Side (top) and top (bottom) view of the tilted WO_6 chains in $Sr_2[WO_5]$ in *Pna*2$_1$ (strontium grey, oxygen red, WO_6 octahedra blue); all atoms are drawn with their displacement ellipsoids at a 95% probability level.

1.82–2.11 Å, 76–102° (adjacent), and 161–173° (opposite), respectively (Table 3).
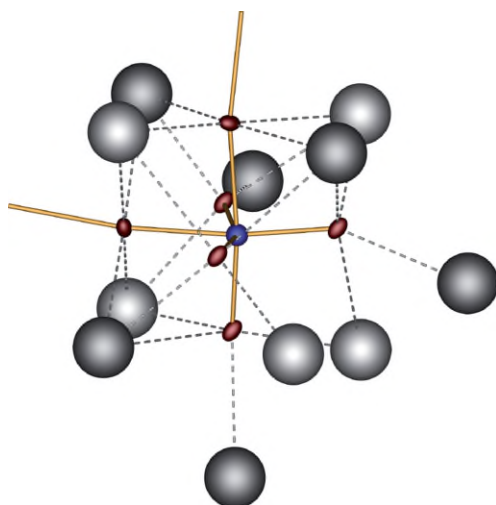
Figure 4. Distortion of the WO_6 octahedra in $Sr_2[WO_5]$ and their strontium coordination. Sr1 dark grey, Sr2 light grey, W1 blue; the oxygen atoms (red) are drawn with their displacement ellipsoids at a 75 % probability level.

Table 3. Relevant ranges of interatomic distances /Å and angles /° in $Sr_2[WO_5]$ in space group $Pna2_1$ (esds in parentheses).

Sr–O	2.455(3)–3.161(5)
W1–O1	2.040(7)–2.112(7)
W1–O2	1.858(3)
W1–O3	1.948(3)
W1–O4	1.829(5)
W1–O5	1.819(5)
O–W–O (adj.)[a]	76.3(2)–101.82(19)
O–W–O (opp.)[a]	161.17(17)–173.2(2)
W–O_{brid}–W [a]	167.8(2)

a) adj. = adjacent neighbors, opp. = opposite neighbors, O_{brid} = bridging oxygen atom.

Both strontium sites are coordinated ten-fold by oxygen atoms. The coordination polyhedra can be described as distorted singly capped triangular cupola (Johnson polyhedron J_3) and distorted sphenocorona (Johnson polyhedron J_{86}) for Sr1 and Sr2, respectively (Figure 5). The Sr–O distances range from 2.45–3.16 Å providing an average of 2.74 Å, which corresponds exactly to the sum of the effective ionic radii according to *Shannon*.[15]
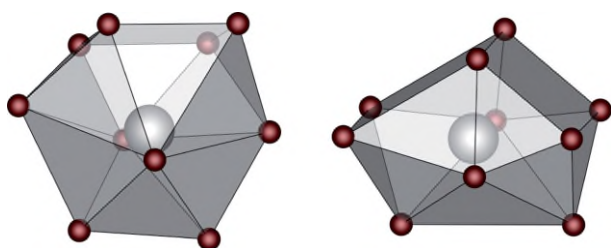
Figure 5. Ten-fold coordination of Sr1 (left) and Sr2 (right) by oxygen atoms in $Sr_2[WO_5]$. Strontium grey, oxygen red.

Validation of the $Ba_2[WO_5]$ Structure

Since *Kovba* et al.[9] published just isotropic displacement parameters for $Ba_2[WO_5]$, we have found it worthwhile to validate the assigned *Pnma* space group. Single-crystals were prepared by the same method as for $Sr_2[WO_5]$ and a data set was measured. As for $Sr_2[WO_5]$, XPREP suggested the space group *Pnma*, but in this case the principal mean square atomic displacements (Table 4) and anisotropic displacement parameters (Table S6, Supporting Information) revealed no conspicuousness.

Table 4. Principal mean square atomic displacements /Å^2 in $Ba_2[WO_5]$.

Atom	$<u_x^2>$	$<u_y^2>$	$<u_z^2>$
Ba1	0.0038	0.0032	0.0024
Ba2	0.0044	0.0032	0.0030
W1	0.0026	0.0022	0.0018
OB	0.0065	0.0059	0.0034
OT1	0.0074	0.0064	0.0038
OT2	0.0070	0.0058	0.0028
OT3	0.0066	0.0056	0.0037

While the overall structural configuration and the cation coordination are very similar to $Sr_2[WO_5]$ (space group $Pna2_1$), there is no tilt in the WO_6 zigzag chain in $Ba_2[WO_5]$ in space group *Pnma* (Figure 6). The out-of-centre distortion of the WO_6 octahedra in $Ba_2[WO_5]$ (Table 5 and Figure 7) is not as pronounced as in $Sr_2[WO_5]$.
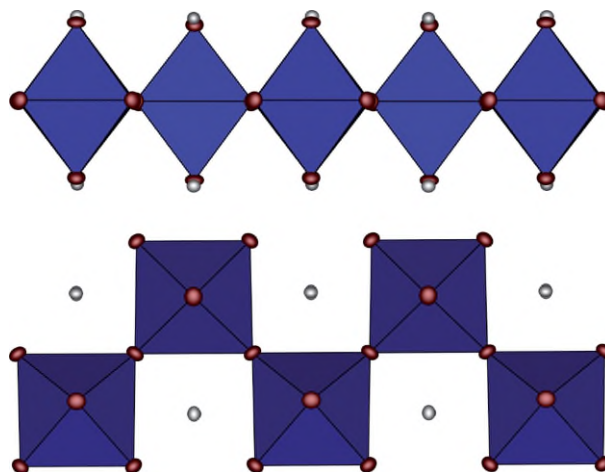
Figure 6. Side (top) and top (bottom) view of the non-tilted WO_6 chains in $Ba_2[WO_5]$ in *Pnma*. Barium grey, oxygen red, WO_6 octahedra blue; all atoms are drawn with their displacement ellipsoids at a 95 % probability level.

Table 5. Relevant ranges of interatomic distances /Å and angles /° in $Ba_2[WO_5]$ in space group *Pnma* (esds in parentheses).

Ba–O	2.622(3)–2.9750(17)
W1–OB	2.08982(9)
W1–OT1	1.860(2)
W1–OT2	1.945(2)
W1–OT3	1.8335(18)
O–W–O (adj.)[a]	84.11(5)–97.42(11)
O–W–O (opp.)[a]	164.47(11)–174.19(6)
W–O_{brid}–W [a]	180

a) adj. = adjacent neighbors, opp. = opposite neighbors, O_{brid} = bridging oxygen atom.
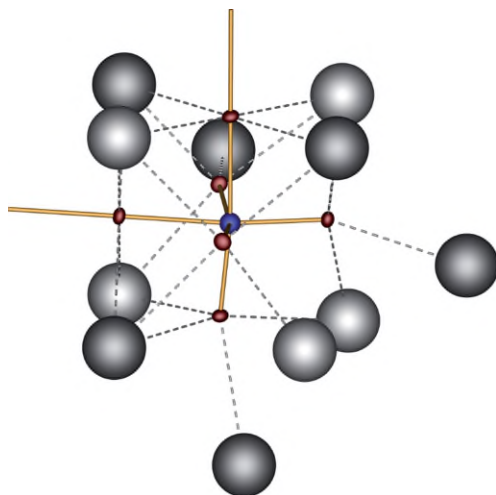
Figure 7. Distortion of the WO_6 octahedra in $Ba_2[WO_5]$ and their barium coordination. Ba1 dark grey, Ba2 light grey, W1 blue; the oxygen atoms (red) are drawn with their displacement ellipsoids at a 75% probability level.

Electrostatic Calculations

We also checked the structure models of $Sr_2[WO_5]$ and $Ba_2[WO_5]$ for electrostatic reasonability using calculations based on the MAPLE concept (MAPLE = Madelung Part of Lattice Energy).[16–18] A structure model is considered as electrostatically consistent if the sum of MAPLE values of chemically similar compounds deviates from the MAPLE value of the compound of interest by less than 1%.

According to our calculations the deviations amount to 1.03% for $Sr_2[WO_5]$ and 0.63% for $Ba_2[WO_5]$. Both structure models thus show electrostatic consistency. SrO (ICSD no. 109461), BaO (ICSD no. 616004) and WO_3 (ICSD no. 16080) were used as binary reference compounds. Details of the calculations are listed in Table S2 (Supporting Information).[19–21]

DFT Calculations

DFT-PBE and hybrid-HSE06 calculations overestimate the lattice parameters for both $Sr_2[WO_5]$ and $Ba_2[WO_5]$, which is very well known and expected (Table S7, Supporting Information). Insulating ground states are obtained for both compounds whereas the bandgaps are slightly underestimated in both cases, although the exact exchange functional HSE06 was used which is usually well performing at correctly describing bandgaps. But the obtained trend is clearly evident, 3.44 eV for the Ba compound and 3.76 eV for the Sr compound. The bonding situation in $Sr_2[WO_5]$ and $Ba_2[WO_5]$ is very similar, which is depicted by atomic site projected densities of states (Figure 8 and Figure 9). The bridging oxygen atom (O1) shows a different characteristic with a higher sharp maximum below E_F. O2 and O3, pointing up- and downwards in the octahedral chains, can be distinguished from other O sites by higher DOS at –2 eV indicating also the shorter bonding distance W–O.
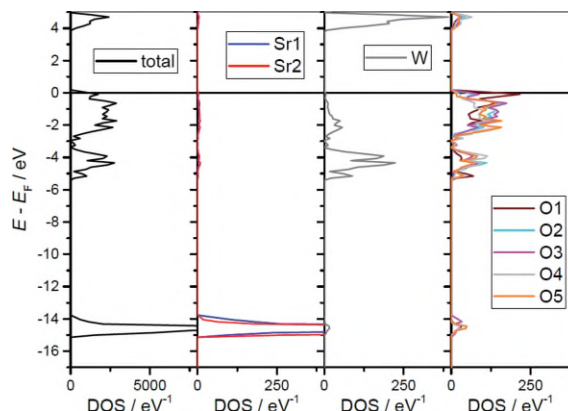
Figure 8. Atomic site projected densities of states (DOS) of $Sr_2[WO_5]$.
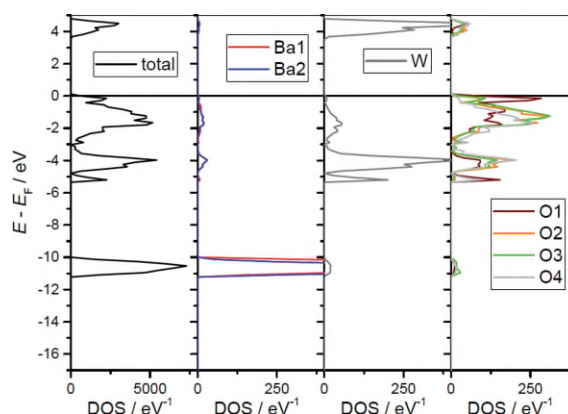
Figure 9. Atomic site projected densities of states (DOS) of $Ba_2[WO_5]$.

Infrared and Raman Spectroscopy

The IR and Raman spectra of $Sr_2[WO_5]$ and $Ba_2[WO_5]$ (Figure 10 and Figure 11) were recorded in the range of 4000–400 cm^{-1} (IR on powder samples) and 1800–35 cm^{-1} (Raman on single-crystals). Above 1000 cm^{-1} no absorption bands were recorded.

The Raman spectrum of $Sr_2[WO_5]$ (Figure 10) comprises a strong symmetric stretching mode of the WO_6 octahedra at 840 cm^{-1}. The asymmetric stretching vibrations lie between 775–500 cm^{-1}, followed below by several bending vibrations. In the IR spectrum, several strong bands in the same regions can be assigned to the same sort of vibrational mode.

In $Ba_2[WO_5]$ (Figure 11) the symmetric stretching vibration is at 820 cm^{-1}, whereas the asymmetric stretching vibrations of the WO_6 octahedra are in the region 750–500 cm^{-1} and the bending vibrations follow below 450 cm^{-1}.

The spectra of both compounds coincide with the data presented by *Poloznikova* et al.[22]

UV/Vis Spectroscopy and Eu³⁺ Fluorescence

The UV/Vis reflectance spectra of the undoped alkaline earth tungstates (Figure 12) reveal one absorption edge each, centred at 334 nm and 319 nm for $Ba_2[WO_5]$ and $Sr_2[WO_5]$,
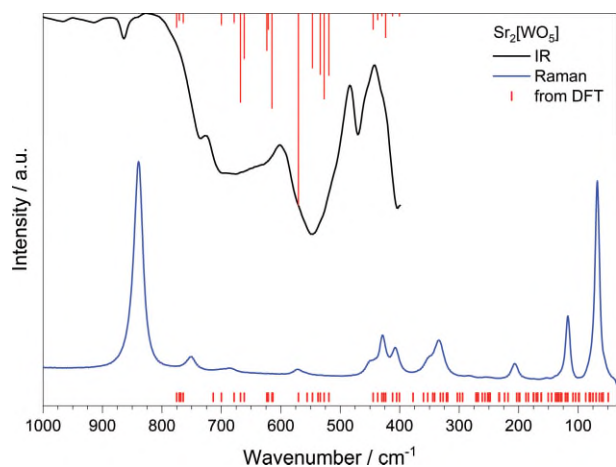
Figure 10. IR (black) and Raman (blue) spectra of $Sr_2[WO_5]$; the red bars represent the respective IR and Raman modes calculated by DFT.
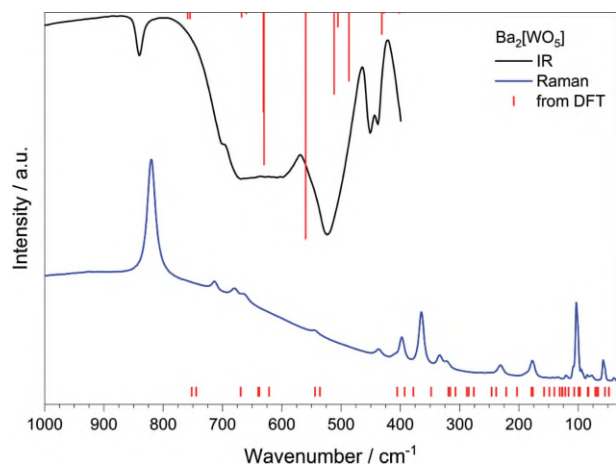
Figure 11. IR (black) and Raman (blue) spectra of $Ba_2[WO_5]$; the red bars represent the respective IR and Raman modes calculated by DFT.

Figure 12. UV/Vis reflectance spectra of undoped $Ba_2[WO_5]$ (blue) and $Sr_2[WO_5]$ (red).

curs via the W–O–*RE* bridges comprising angles of 148.0° (O4), 151.8° (O5), and 159.0° (O3). Attempts to reduce Eu^{3+} to Eu^{2+} resulted in the formation of dark colored tungsten bronzes not showing any fluorescence.
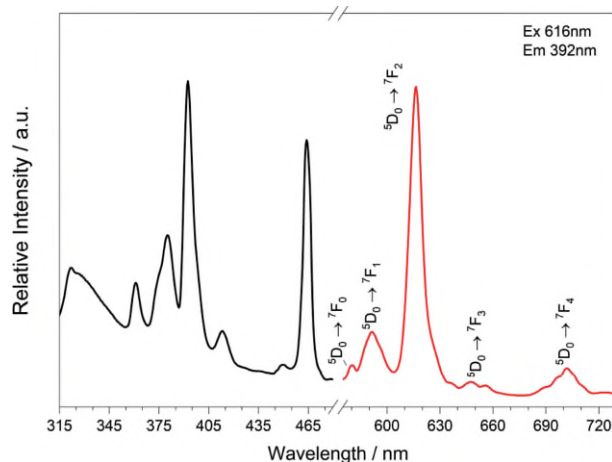
Figure 13. Absorption (black) and emission (red) spectra of Eu^{3+} doped $Sr_2[WO_5]$.

respectively. Thus the optical bandgap is expected at approximately 3.9 eV for $Ba_2[WO_5]$ and 4.0 eV for $Sr_2[WO_5]$. These results are astonishing on first glance but are well supported by the DFT calculations. The electronegativity values of Sr and Ba are comparable with Sr being the slightly more electronegative element. The closest W–W contacts are shorter (4.13 Å) in the strontium compound compared with the barium compound (4.18 Å); in both cases the bridging oxygen atom is surrounded by two tungsten and four alkaline-earth atoms. Thus, slightly more electron density is apparently withdrawn from the bridging oxygen atom in the strontium compound leading to a weaker W–O–W bridge and accordingly a stronger repulsion of adjacent tungsten atoms – yielding a slightly larger band-gap in the strontium compound.

Although most W–O–Sr angles are close to 90° (in the range of 78.6–119.7° with a mean value of 93.6°, Figure 4), which is not favorable in terms of an effective energy transfer from the tungstate to the rare earth activator ion,[6] we have observed strong red-orange Eu^{3+} luminescence (Figure 13) upon incorporation of 2 mol % $Eu(NO_3)_3 \cdot 5H_2O$ during the synthesis of $Sr_2[WO_5]$. Thus, probably, most of the energy transfer oc-

Conclusions

In our study we shed more light on the crystal structures of $Ba_2[WO_5]$ and $Sr_2[WO_5]$ solving the problem of the extremely large displacement parameters found for the strontium compound by reducing the symmetry and introducing the respective twin law. The proper space group is apparently *Pna2₁* for $Sr_2[WO_5]$ allowing for an ordered tilting of the zigzag chain of condensed WO_6 octahedra. In contrast to the strontium compound, the barium compound crystallizes indeed in space group *Pnma* as determined previously yielding linear bridges and no tilting of the chain.

Presumably the stronger repulsion of adjacent "W^{6+}" ions is larger in $Sr_2[WO_5]$ and the atomic arrangement does not fit that well with the sizes of Sr/W like in the case of $Ba_2[WO_5]$.

This effect also seem to be responsible for the larger bandgap observed in this study for $Sr_2[WO_5]$. The trend was confirmed by DFT calculations which also helped us to identify the assignment of vibrational frequencies found in both title compounds. Looking at the W–O vibrations, these show a shift to smaller energies in the barium compound with respect to the strontium compound what is in accordance with weaker W–O interactions as concluded from the discussion of the different band-gap energies of both compounds. Considering the doped $Sr_2[WO_5]$:Eu^{3+} an energy transfer from the tungstate groups seems to occur reflected in the broad excitation band around 325 nm close to the absorption edge – although the most effective excitation for the main emission wavelength remains the *4f–4f* transition around 381 nm for the strongest red-orange $^5D_0 \rightarrow {}^7F_2$ emission.

Experimental Section

Synthesis: Polycrystalline powder of $Sr_2[WO_5]$ was obtained from the solid state reaction of $Sr(NO_3)_2$ (655.8 mg, $\geq$ 99 %, Fluka) and WO_3 (343.3 mg, 99.9 %, Fluka) at 1100 °C in air. The reaction mixture was fired in an electrical furnace for 78 h with one intermediate grinding step, using a platinum crucible. The phase purity was checked by powder X-ray diffraction (Figure S1, Supporting Information).

Single-crystals of $Sr_2[WO_5]$ were obtained from the reaction of $SrWO_4$ and SrF_2 in the molar ratio of 2:3 in a platinum crucible. The mixture of starting materials was heated in air, according to the following temperature program: heat to 900 °C with 100 K·h^{-1}, hold 10 min, heat to 1200 °C with 5 K·h^{-1}, hold 12 h, cool to room temperature with 100 K·h^{-1}.

$SrWO_4$ was prepared from $SrCO_3$ (96.0 %, Riedel-de Haën) and WO_3, SrF_2 from $SrCl_2 \cdot 6H_2O$ (99.00 %, Aldrich) and NH_4F (p.a., Acros).

For doping of $Sr_2[WO_5]$ with Eu^{3+}, a mixture of $(1–x)Sr_2WO_5$, $xSrWO_4$ and $xEu(NO_3)_3 \cdot 5H_2O$ was heated at 1000 °C for 24 h.

Polycrystalline powder of $Ba_2[WO_5]$ was obtained from $BaCO_3$ (635.7 mg, 99+ %, Aldrich) and WO_3 (364.5 mg, 99.9 %, Fluka) in air. After thoroughly grinding the reaction mixture, it was heated in a platinum crucible to 1150 °C with a heating rate of 100 K·h^{-1}, held at this temperature for 24 h and cooled to room temperature with 100 K·h^{-1}. The phase purity was checked by powder X-ray diffraction (Figure S2, Supporting Information). Single-crystals of $Ba_2[WO_5]$ were obtained from the reaction of $BaWO_4$ and BaF_2 in the molar ratio of 2:3 in a platinum crucible. The reaction mixture was fired in air at 1000 °C for 24 h with heating and cooling rates of 100 K·h^{-1}.

Crystal Structure Determination: Suitable crystals of $Sr_2[WO_5]$ and $Ba_2[WO_5]$ were selected under a optical microscope and cooled to 100 K at a rate of 25 K·h^{-1}. Single-crystal X-ray diffraction data were collected with a Bruker D8 Venture diffractometer equipped with a SMART APEXII 4k CCD detector, using Mo-K_α radiation; the data were corrected for absorption by applying a multi-scan approach. The crystal structures were solved by intrinsic phasing ($Sr_2[WO_5]$) and direct methods ($Ba_2[WO_5]$), respectively, and refined using the SHELXTL program package[23] with anisotropic displacement parameters for all atoms. Details of the X-ray data collection are summarized in Table 6. The positional and displacement parameters for all atoms are listed in the Supporting Information (Tables S3 to S6).

Table 6. Crystal data and details of structure refinements.

	$Sr_2[WO_5]$	$Ba_2[WO_5]$
Temperature /K	100(2)	100(2)
M /g·mol^{-1}	439.09	538.53
Crystal system	orthorhombic	orthorhombic
Space group	$Pna2_1$ (no. 33)	$Pnma$ (no. 62)
a /Å	7.2457(3)	7.3828(2)
b /Å	10.8867(5)	5.71420(10)
c /Å	5.5391(3)	11.4701(3)
V /Å^3	436.93(4)	483.89(2)
Z	4	4
ρ X-ray /g·cm^{-3}	6.675	7.392
Crystal dimensions /mm^3	$0.020 \times 0.015 \times 0.010$	$0.125 \times 0.035 \times 0.015$
Color and shape	colorless block	colorless block
μ /mm^{-1}	50.500	39.730
$F(000)$	760	904
Radiation, λ /Å	Mo-K_α (0.71073)	Mo-K_α (0.71073)
Diffractometer	Bruker D8 Venture	Bruker D8 Venture
Abs. corr.	multi-scan	multi-scan
Min. / max. transmission	0.5536 / 0.7489	0.3802 / 0.7503
Index range	±14 / ±21 / ±10	–11 / –9 / –18 / –11 / 8 / 18
Theta range	2.811–44.994	3.282–34.988
No. coll. refl. / Ind. data	40652 / 3587	9769 / 1142
Parameter / Restraints	56 / 1	47 / 0
Obs. refl. (I $> 2\sigma$) / R_{int}	2878 / 0.0671	1118 / 0.0294
R (all data)	$R_1 = 0.0495$, $wR_2 = 0.0462$	$R_1 = 0.0146$, $wR_2 = 0.0284$
Weighting scheme	$w^{-1} = \sigma^2 F_o^2 + (0.0177 P)^2 + 0.7658 P$; $P = (F_o^2 + 2F_c^2)/3$	$w^{-1} = \sigma^2 F_o^2 + (0.0076 P)^2 + 0.8602 P$; $P = (F_o^2 + 2F_c^2)/3$
GooF	1.072	1.250
Twin refinement / BASF	(1 0 0)(0 1 0)(0 0 –1) / 0.49(3)	n. a.
Min. / max. res. density /e$^-$·Å^{-3}	–1.96 / 3.61	–2.40 / 1.05

Further details of the crystal structures investigations may be obtained from the Fachinformationszentrum Karlsruhe, 76344 Eggenstein-Leopoldshafen, Germany (Fax: +49-7247-808-666; E-Mail: crysdata@fiz-karlsruhe.de, http://www.fiz-karlsruhe.de/request for deposited data.html) on quoting the depository numbers CSD-433567 ($Sr_2[WO_5]$ and CSD-433568 ($Ba_2[WO_5]$)).

Powder X-ray Diffraction: The phase purity of the powder samples of $Sr_2[WO_5]$ and $Ba_2[WO_5]$ was checked by powder X-ray diffraction (Figures S1 and S2, Supporting Information). The pattern was recorded with a Seifert XRD T/T 3003 diffractometer in reflection geometry equipped with a Meteor 1D linear detector.

Density Functional Theory Calculations: Quantum chemical calculations were performed in the framework of density functional theory (DFT) using a linear combination of Gaussian-type functions (LCGTF) Scheme as implemented in CRYSTAL14.[24,25] The total energy calculations including full structural optimizations and subsequent calculations of the vibrational frequencies were performed with the GGA (PBE)[26] xc-functional. Furthermore, electronic structures were tested by the calculations including full structural relaxations with the exact exchange functional HSE06[27,28] which includes a Hartree-Fock term in the exchange part. The convergence criterion considering the energy

was set to 1×10^{-8} a.u. with a *k*-mesh sampling of $8 \times 8 \times 8$ for both compounds. Optimized effective core potential basis sets were applied for Sr, Ba, and W,[29–31] the description of the oxygen atoms was carried out by an all-electron basis.[32] Vibrational frequencies calculations with IR intensities were run on fully optimized structural models so that no imaginary frequency was obtained. For the Raman spectra, only the band positions were calculated. The modes were visualized and analysed with the J-ICE application.[33] The optimized cell parameters obtained by DFT calculations are listed in Table S7 (Supporting Information).

Spectroscopy: IR spectra were recorded with a Bruker EQUINOX 55 FT-IR Spectrometer equipped with a Platinum ATR unit in the range 4000–400 cm^{-1} with a resolution of 2 cm^{-1} and 64 scans. Raman spectra were recorded with a Thermo Scientific DXR Raman-Microscope in the range 1800–35 cm^{-1} using a 532 nm laser operated with 10 mW power (10–fold magnification, 50 µm pinhole aperture, high resolution grating (1800 lines mm^{-1}), spectral resolution (1 cm^{-1}). UV/Vis spectra were recorded in reflection geometry with a Varian Cary 300 Scan UV/Vis spectrometer. Fluorescence absorption and emission spectra were recorded with a Horiba Fluoromax-4 spectrometer, scanning a range from 250 to 800 nm.

Supporting Information (see footnote on the first page of this article): tables containing the refined coordinates as well as the respective thermal displacement parameters, powder diffraction patterns and tables containing the results of the theoretical calculations.

Acknowledgements

Keywords: Strontium; Tungsten; Barium; Tungstate

References

[1] H. A. Höppe, *Angew. Chem. Int. Ed.* **2009**, *48*, 3572.
[2] H. A. Höppe, S. J. Sedlmaier, *Inorg. Chem.* **2007**, *46*, 3467.
[3] H. A. Höppe, *J. Solid State Chem.* **2009**, *182*, 1786.
[4] H. A. Höppe, K. Kazmierczak, S. Kacprzak, I. Schellenberg, R. Pöttgen, *Dalton Trans.* **2011**, *40*, 9971.
[5] M. Daub, A. J. Lehner, H. A. Höppe, *Dalton Trans.* **2012**, *41*, 12121.
[6] G. Blasse, A. Bril, *J. Chem. Phys.* **1966**, *45*, 2350.
[7] M. Keskar, S. K. Sali, B. G. Vats, R. Phatak, K. Krishnan, S. Kannan, *J. Alloys Compd.* **2017**, *695*, 3639.
[8] N. Shevchenko, L. Lykova, L. Kovba, *Russ. J. Inorg. Chem.* **1974**, *19*, 528.
[9] L. Kovba, L. Lykova, V. Balashov, A. Kharlanov, *Koord. Khim.* **1985**, *11*, 1426.
[10] M. Gateshki, J. M. Igartua, *J. Phys.: Condens. Matter* **2004**, *16*, 6639.
[11] M. Gateshki, *Dissertation*, Euskal Herriko Unibertsitatea, Leioa, Spain, **200**.
[12] R. R. Ryan, S. H. Mastin, M. J. Reisfeld, *Acta Crystallogr., Sect. B* **1971**, *27*, 1270.
[13] *PDF-2*, Release 2000, International Centre for Diffraction Data, **2000**.
[14] M. Kunz, I. D. Brown, *J. Solid State Chem.* **1995**, *115*, 395.
[15] R. D. Shannon, *Acta Crystallogr., Sect. B* **1976**, *32*, 751.
[16] R. Hoppe, *Angew. Chem. Int. Ed. Engl.* **1966**, *5*, 95.
[17] R. Hoppe, *Angew. Chem. Int. Ed. Engl.* **1970**, *9*, 25.
[18] R. Hübenthal, *MAPLE*, Program for the Calculation of the Madelung Part of Lattice Energy, Gießen, Germany, **1993**.
[19] J. Bashir, R. T. A. Khana, N. M. Butt, G. Heger, *Powder Diffr.* **2002**, *17*, 222.
[20] R. J. Zollweg, *Phys. Rev.* **1955**, *100*, 671.
[21] B. O. Loopstra, H. M. Rietveld, *Acta Crystallogr., Sect. B* **1969**, *25*, 1420.
[22] M. Poloznikova, A. Kabakchi, V. Balashov, O. Kondratov, V. Fomichev, *Zh. Neorganicheskoi Khim.* **1990**, *35*, 802.
[23] G. Sheldrick, *Acta Crystallogr., Sect. A* **2008**, *64*, 112.
[24] R. Dovesi, V. R. Saunders, C. Roetti, R. Orlando, C. M. Zicovich-Wilson, F. Pascale, B. Civalleri, K. Doll, N. M. Harrison, I. J. Bush, P. D'Arco, M. Llunell, M. Causà, Y. Noël, *CRYSTAL14*, User's Manual, University of Torino, Torino, Italy, **2014**.
[25] R. Dovesi, R. Orlando, A. Erba, C. M. Zicovich-Wilson, B. Civalleri, S. Casassa, L. Maschio, M. Ferrabone, M. D. L. Pierre, P. D'Arco, Y. Noël, M. Causà, M. Rérat, B. Kirtman, *Int. J. Quantum Chem.* **2014**, *114*, 1287.
[26] J. P. Perdew, K. Burke, M. Ernzerhof, *Phys. Rev. Lett.* **1996**, *77*, 3865.
[27] A. D. Becke, *Phys. Rev. A* **1988**, *38*, 3098.
[28] J. Heyd, G. E. Scuseria, M. Ernzerhof, *J. Chem. Phys.* **2003**, *118*, 8207.
[29] S. Piskunov, E. Heifets, R. I. Eglitis, G. Borstel, *Comput. Mater. Sci.* **2004**, *29*, 165.
[30] A. Mahmoud, A. Erba, K. E. El-Kelany, M. Rérat, R. Orlando, *Phys. Rev. B* **2014**, *89*, 045103.
[31] Basis set ECP60MHF for W, ECP60MHF, http://www.tc.uni-koeln.de/PP/clickpse.en.html.
[32] J. Scaranto, S. Giorgianni, *J. Mol. Struct.* **2008**, *858*, 72.
[33] P. Canepa, R. M. Hanson, P. Ugliengo, M. Alfredsson, *J. Appl. Crystallogr.* **2014**, *47*, 225.
[34] J. M. Igartua, Universidad del País Vasco / Euskal Herriko Unibertsitatea, private communication.